

RESEARCH NOTE

Copy edited by JRS: 2/6/12

A note on the pure katabatic wind maximum over gentle slopesBranko Grisogono¹ and Simon L. Axelsen²

AMGI Dept. of Geophysics, Faculty of Sci. & Math., Univ. of Zagreb, Horvatovac 95, 10000 Zagreb,

Croatia

Received: 23 November 2011

Accepted: 5 June 2012

Abstract

The wind maximum of pure katabatic winds over moderate slopes, the inclination varying between 3 to 6°, is studied using large-eddy simulation (LES) and further discussed in the light of the classical Prandtl model. The LES results show that both the maximum katabatic wind speed and its height decrease with increasing slope angle, and vice versa. However, in the Prandtl analytical, i.e. linear classical, solution, only the wind maximum height is affected by the slope angle, not the maximum wind speed. For the given range of slope inclinations, a linear relation between the height and the magnitude of the wind maximum is found in our simulations, which is supported by a limited dataset obtained by other researchers; these results are further discussed. The inability of the analytical Prandtl solution to give the maximum wind-speed dependency on the slope angle is associated with the assumed constancy of, 1) the background vertical potential temperature gradient Γ , 2) the eddy diffusivity and 3) the Prandtl number.

Key Words: Large-eddy simulation ; Low-level jet; Prandtl model; Stratified turbulence

1 Introduction

This note assesses one basic aspect of simple katabatic flows, namely, the dependency of the katabatic low-level jet (LLJ) on the value of a constant slope angle. Being of theoretical interest, this problem is important from parametrization perspectives since most climate models do not resolve katabatic flows. Even numerical weather prediction (NWP) and mesoscale models may have problems in simulating

¹ The corresponding author, bgrisog@gfz.hr
² simon.axelsen@gmail.com

Scanned & sent to Deepansh 5/6/12
 cc. authors

30 katabatic flows adequately (e.g. Renfrew 2004; Renfrew and Anderson 2006; Grisogono and Belušić
31 2008). Hence, this type of flow remains in the research focus for experimentalists and modellers, e.g.
32 Cuxart and Jiménez (2007), Rotach and Zardi (2007). Katabatic flows are important in determining or
33 modulating e.g. mountainous microclimate and the future of glaciers (e.g. Oerlemans et al. 1999);
34 furthermore, there are implications that katabatic flows contribute to the general atmospheric
35 circulation (Parish and Bromwich 1991). On a finer scale, Largeron et al. (2010) found that the eddy
36 diffusivity related to the katabatic flow is proportional to the corresponding Froude number squared,
37 and that this diffusivity evolves linearly in time during the first few hours of the flow evolution. Next,
38 katabatic winds may generate buoyancy waves; furthermore, the stratification is partly produced by the
39 katabatic flow itself (e.g. Chemel et al. 2009).

40

41 Some research related to the dependency of katabatic wind profiles on the slope angle has been
42 published, yet the focus has not been ~~put~~ on the wind maximum and its height as functions of the
43 (single) slope inclination. Previous work has presented results from which this dependency could be
44 loosely deduced or guessed. For example, Heilman and Talke (1991), using a second-order closure
45 model, found that the maximum katabatic speed slightly increases with decreasing slope angle, but the
46 corresponding LLJ height increases more markedly for larger slope inclinations. Haiden and
47 Whiteman (2005) studied katabatic flow down a 1.6° slope experimentally and found, for a weaker
48 ambient stratification, katabatic flow acceleration between two sites to be larger than that predicted
49 based on observed buoyancy. Numerical simulations by Smith and Skillingstad (2005), who used
50 large-eddy simulation (LES) and a mesoscale model with ^{spatial} very high resolution, qualitatively suggest
51 that the magnitude and the corresponding height of the katabatic wind maximum may increase slightly
52 with decreasing slope angle (they studied a composite slope flow, from a larger to a smaller angle).
53 Cuxart and Jiménez (2007), in a complex approach to katabatic and drainage flows, also used LES to
54 assess the flow budgets and mixing processes. Zhong and Whiteman (2008) found, using another
55 mesoscale model, that the downslope flow is stronger above the gentle slope, and deeper on the steep
56 slope; the latter perhaps also means that the elevation of the maximum wind speed, i.e. the LLJ,
57 increases over the steep slope in their results. Hence, the effect of constant slope angle on the related
58 LLJ is not a settled issue; this note makes a contribution by addressing the pure katabatic wind
59 maximum over constant gentle slopes.

60

61 Classical Prandtl (linear) theory (Prandtl 1942; Egger 1990; Grisogono and Oerlemans 2001a; b)
62 provides the maximum speed of the katabatic flow as independent of the slope angle, while the height
63 of the katabatic jet, i.e. the LLJ, according to the same theory, is inversely proportional to the square
64 root of the sine of the slope angle (e.g. Grisogono and Oerlemans 2001b, 2002; Parmhed et al. 2004).
65 The elegance and scientific essence of the Prandtl model is that it couples basic dynamics and
66 thermodynamics for inclined surfaces in the most succinct way. The dependency of the pure katabatic
67 LLJ on the slope angle is the aim of this study. Note that an arguably simpler model for pure katabatic
68 flows, parametrizing turbulent friction in the simplest possible way as being proportional to the wind
69 speed (with the opposite sign than the speed), yields the katabatic wind speed that is inversely
70 proportional to the sine of the slope angle (e.g. Petkovšek and Hočevár 1971).

71

72 We address the pure katabatic wind maximum and its position, i.e., the basic katabatic LLJ, by LES
73 and analytic reasoning related to the Prandtl model (e.g. Axelsen and Van Dop 2009a, b; Burkholder et
74 al. 2009). The approach is chosen because it is difficult to measure in reality the exact position, and
75 thus the maximum speed, of very low katabatic jets; when these occur at, say, 3 to 8 m height where
76 virtually any small terrain inhomogeneity and cross-slope variability may induce significant flow
77 variations, data spatial representativity and three-dimensional effects may easily contaminate the
78 intended observations. Meanwhile, computational resources have progressed and improved
79 sufficiently nowadays, so that many properties of the stable boundary layer become gradually revealed
80 by using e.g. LES and even more advanced numerical methods (e.g. Smith and Skillingstad 2005; Van
81 Dop and Axelsen 2007; Cuxart and Jiménez 2007; Axelsen and Van Dop 2009a, b; Fedorovich and
82 Shapiro 2009). This study follows Grisogono and Oerlemans (2001a, b; 2002), Smith and Skillingstad
83 (2005) and Axelsen and Van Dop (2009a, b), and in the following, we present the analytical and
84 numerical models, and discuss results. A weakness of the linear Prandtl model, i.e. its maximum wind-
85 speed indifference regarding the slope angle, is discussed; moreover, we offer concluding remarks.

86

87

88 2 Analytical and numerical models

89

90 We start with a more general but still simplified equation set; then we will finish with the Prandtl
 91 model allowing for analytical solutions on the one hand, and on the other hand, with a deployment of a
 92 rather general LES model permitting solely numerical solutions. For brevity, we only give the flavour
 93 of deriving the Prandtl model, whose basis is the set of conservation equations for thermodynamic
 94 energy and momentum. These equations, without Coriolis effects, expressed in a slope parallel
 95 coordinate system with axes x_i , which point in the downslope, cross-slope and slope normal directions,
 96 respectively, are (e.g. Denby 1999, Axelsen and Van Dop 2009a):

$$98 \quad \frac{D\theta}{Dt} = \Gamma(u_1 \sin \alpha - u_3 \cos \alpha) + \frac{\partial}{\partial x_j} (K_H \frac{\partial \theta}{\partial x_j}), \quad (1)$$

$$100 \quad \frac{Du_i}{Dt} = -\frac{1}{\rho_0} \frac{\partial p}{\partial x_i} - \frac{g\theta}{\Theta_0} (\delta_{1i} \sin \alpha - \delta_{3i} \cos \alpha) + \frac{\partial}{\partial x_j} (K_M \frac{\partial u_i}{\partial x_j}), \quad (2)$$

101
 102 where the former has been expressed in terms of the potential temperature difference between the air
 103 participating in the flow and the ambient quiescent atmosphere. The three components of the induced
 104 velocity vector (u, v, w) are denoted by u_i , and point in the direction of x_i , Θ_0 is a constant reference
 105 potential temperature and $\Gamma \equiv d\Theta/dz^*$ is the rate of change of environmental potential temperature Θ_e
 106 along the direction z^* of the gravity vector. Moreover, p and ρ_0 are the pressure field and a reference
 107 density, while K_H and K_M are parametrizations for the eddy heat conductivity and eddy diffusivity³,
 108 respectively. On the left-hand sides, there are altogether (i.e. in a Lagrangian sense), the local rate of
 109 changes and the non-linear advective changes of θ and u_i , respectively. The latter contributions,
 110 together with the nearly-horizontal pressure gradient, will usually be neglected in the Prandtl model.

111
 112 The Prandtl model is best used over a long and uniformly tilted surface with relatively small slope
 113 angle α (say, $\alpha \approx 10^\circ$ and less), although there is no direct restriction to α ; it assumes Boussinesq
 114 approximation and a “quasi-hydrostatic” ambient atmosphere that considers the relationship between

³ The related turbulent processes are largely resolved in LES models, i.e. the most energetic eddies are calculated explicitly; hence, there is no basic need for such parametrization using K_{HM} in the latter models. However, the so-called sub-filter scale fluxes, ~~that~~ are supposed to contribute relatively little to total (resolved and unresolved) fluxes, in LES are often parametrized via ~~form~~ of “K-theory”.

a kind

the slope and hydrostatic assumption in a succinct way (Mahrt 1982; Haiden 2003). The related equations (see the next set) are apparently valid even at large angles, say $\alpha \rightarrow \pi/2$ since the slope is (naively) infinitely long in this model (however, subtle details about the appropriate use of the hydrostatic assumption and the full tensor coordinate transformations, and vice versa, can be found in e.g. Pielke 1984). The last terms on the right-hand sides of (1) and (2) are dominated by the slope perpendicular (upward) variations, i.e. these are due to $\partial/\partial x_j \rightarrow \partial/\partial z$ variations.

In order to produce a straightforward analytical solution, it is assumed in the Prandtl model that the flow is solely along a constant slope, stationary and invariant in the downslope direction, i.e. $\partial/\partial t = 0$, and $\partial/\partial x = 0$, respectively. Moreover, for simplicity there is no motion in the y -direction (this could be relaxed as in e.g. Kavčič and Grisogono 2007; Shapiro and Fedorovich 2008). Keeping the eddy diffusivities constant, the essential dynamics of the Prandtl model balances negative buoyancy downslope acceleration with frictional retardation due to (very simplified) turbulence effects. The thermodynamic equation expresses a balance between the turbulent heat transport toward the surface and adiabatic warming due to (along-slope) advection of the background temperature gradient. Hence, the resulting set of the very simplified equations becomes, as in e.g. Egger (1990) or Grisogono and Oerlemans (2001a, b; for $\alpha < 0$):

$$\Gamma u \sin \alpha = K_H \frac{d^2 \theta}{dz^2} \quad (3a)$$

and

$$\frac{g\theta}{\theta_0} \sin \alpha = -K_M \frac{d^2 u}{dz^2}. \quad (3b)$$

Assuming the turbulent Prandtl number $Pr = K_M/K_H$ is a constant consequent on the former assumptions deployed, the Prandtl solution, i.e. exponentially-decaying trigonometric functions, then simply reads

$$\theta(z) = C \exp(-\sigma_e z) \cos(\sigma_e z), \quad (4)$$

143 and

144

145
$$u(z) = -C \left[\frac{g}{\Theta_0 \Gamma Pr} \right]^{1/2} \exp(-\sigma_c z) \sin(\sigma_c z), \quad (5)$$

146

147 with $\sigma_c^2 = \frac{\sigma_0}{2K_H} = h^{-2}$, $\sigma_0^2 = g\Gamma \sin^2 \alpha / (\Theta_0 Pr)$, and $C = \theta(z=0) < 0$, as the thermodynamic

148 lower boundary condition, where C is always negative for katabatic flows. The no-slip lower dynamic

149 boundary condition is used for velocity; furthermore, both finite-amplitude perturbations (θ, u)

150 disappear at infinity, $z \rightarrow \infty$. In these exponentially decaying solutions, (4) and (5), as with the Ekman

151 solutions, σ_c plays the role of the vertical wavenumber, or the inverse of the characteristic flow depth

152 for the Prandtl layer, h . Note that h is proportional to $\sin^{-1/2}(\alpha)$; moreover, h is directly proportional to

153 the classic Prandtl LLJ height, i.e. the Prandtl $z_j = \pi h/4$ (e.g. Egger 1990; Grisogono and Oerlemans

154 2001b). Moreover, in the classical Prandtl model the slope angle α should not be zero either, although

155 the model does not show this explicitly since it is not originally derived using a complete tensor

156 coordinate transformation after initially applying all the assumptions considered, which is invariably

157 the rigorous and appropriate way to transform the governing equations into a new coordinate system

158 (e.g. Pielke 1984).

159

160 A more complete picture of turbulent katabatic winds can be obtained using advanced numerical

161 methods; LES is our numerical approach. In LES the motions of the most turbulent eddies, which are,

162 generally speaking, governed by (1) and (2), are resolved explicitly, whereas only small eddies are

163 parametrized. To be more precise, the LES model solves the evolution of the filtered Navier-Stokes

164 equations, thermodynamic energy equation and the Boussinesq form of the conservation of mass. Sub-

165 filtered quantities are parametrized; there, the filter width should be (at least somewhat) larger than the

166 grid-cell size (e.g. Esau 2004; Axelsen and Van Dop 2009a, b). As in the latter, version v3 of the

167 Dutch atmospheric LES model (so-called DALES) is used. The filtered equations are solved on an

168 Arakawa C-grid, a sponge layer emulates a radiative upper boundary condition while in the lateral

169 directions cyclic boundary conditions are used for u_i and θ . A sixth-order spatial discretization of the

170 advection terms and a third-order Runge-Kutta time integration scheme are deployed. Diffusion terms

$(1 \propto 1)$

la.

are treated via second-order central difference scheme. Further details of this LES model used are extensively documented in Axelsen and Van Dop (2009a, b). ^{As articles,} ~~Like in the latter papers,~~ the LES model is suited for simulating katabatic flows pertaining to the class of Prandtl-like gravity flows (Mahrt 1982) where negative buoyancy is largely retarded by turbulent friction, see (3) through (5).

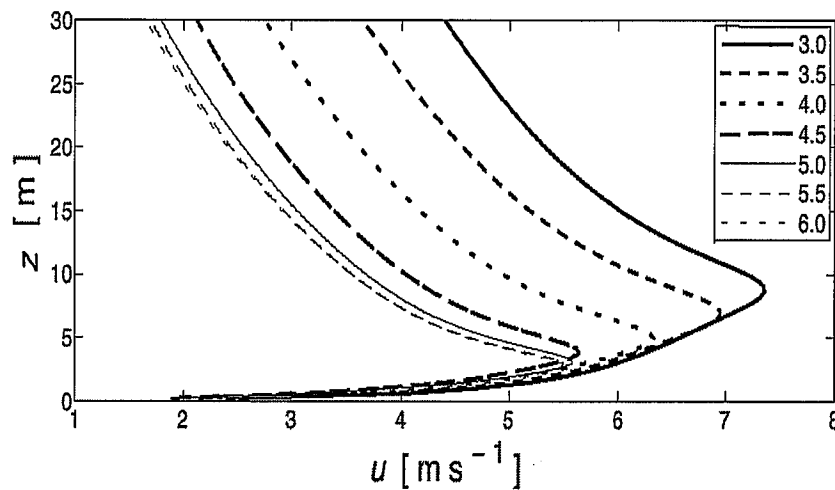
The katabatic flow is simulated via the LES model on a mesh with 128^3 gridpoints with 2.0 and 0.4 m horizontal and vertical (before rotating the frame) spacings, respectively. The simulations are continued until a nearly steady-state is reached, i.e. the simulations proceed until $t = 3\tau$ where $\tau = 2\pi (N \sin \alpha)^{-1}$, $N = (g\Gamma/\Theta_0)^{1/2}$ being the buoyancy frequency, is the oscillation period of katabatic fows (e.g. Mahrt 1982; Schumann, 1990; Grisogono 2003; Fedorovich and Shapiro 2009; Largeron et al. 2010). Then the results are averaged over the last, i.e. third characteristic, period τ during which the oscillations have quite faded away. This is also in agreement with Chemel et al. (2009). Furthermore, the results are averaged along the downslope direction; hence, there is no (t, x) dependency in the results that will be presented. In the only contrast to Axelsen and Van Dop (2009a, b), who forced the katabatic flow using a negative surface heat flux, we prescribe here a constant negative surface potential temperature deficit, i.e. $C = -10$ K, as the lower boundary condition for the potential temperature, and have further used $\Gamma = 3 \text{ K km}^{-1}$. In this way, the LES model set-up is adjusted to treat pure katabatic flows under the same forcings as the Prandtl model, as close as possible. In other words, for the given constant slope, background stratification, eddy conductivity, Pr and the surface potential temperature deficit, unique solutions should ensue for the wind field and temperature in both models (Prandtl and LES). Since the main purpose of this note is to investigate the effect of the slope angle on the steady-state pure katabatic wind, we have varied α from 3° to 6° with increments of half a degree. The aerodynamic roughness length in the LES is constant and equal to 0.01 m.

3 Results and discussion

3.1. LES results

Because of this laboratory-like approach, related to surface-cooled induced flow in a stably-stratified, quiescent atmosphere, one may present results in a very basic and straightforward way. The LES

201 results are illustrated in Figures 1 through 3, and the key results are presented in Table 1. Figure 1
 202 shows that all velocity profiles have the same shape: a sharp increase in u immediately above the
 203 surface, a maximum, and subsequently a somewhat less sharp decrease in u above the maximum. The
 204 magnitude and height of the wind maximum, on the other hand, show for the small slope angles
 205 considered a significant dependency on α . The figure also shows for the two simulations with the
 206 largest slope angles here, $\alpha = 5.5$ and 6° , that the profiles of u overlap almost perfectly.
 207



208
 209 **Figure 1.** Profiles of the katabatic (downslope) flow speed u versus the height z obtained via LES
 210 model. Slope angles ^{are shown and} vary between 3.0 and 6.0 degrees, $C_p = 0.10$ K, $\Gamma = 3$ K km⁻¹. ^{the}

211
 212 Although we are discussing the steady-state of a pure katabatic jet, it is worth mentioning that ^{located}
 213 during the onset of the katabatic flow, which begins at the ~~very~~ surface (where the forcing is), the ^h
 214 dominant eddies are comparable in size to the (initially growing) height of the LLJ. This size
 215 relation changes before time $\approx \tau$ is reached. After steady state is achieved in all seven LES
 216 conducted here, the dominant eddy sizes below z_j are small compared to z_j . This is so because of the
 217 extremely strong near-surface static stability of ~~4~~ 4 to 8 K in the lowest 3 to 8 m; furthermore, the [?]
 218 vertical turbulent momentum flux vanishes at the LLJ nose and reverses its sign above the LLJ in
 219 agreement with Van den Broeke (1997), Van der Avoird and Duynkerke (1999), Grisogono and
 220 Oerlemans (2002), Oerlemans and Grisogono (2002), Parmhed et al. (2004), Cuxart and Jiménez
 221 (2007) and Axelsen and Van Dop (2009a, b). In this way, the LLJ often effectively decouples itself
 222 from the rest of the flow and thus becomes a robust and rather permanent feature of the cooled inclined

microclimate.

Table 1. The simulated katabatic wind maximum u_m and its height z_j (the LLJ height) for various slope angles α . The LLJ height is the value of the grid level at which u_m is found; due to the grid spacing in the LES of 0.4 m, only one decimal can be provided.

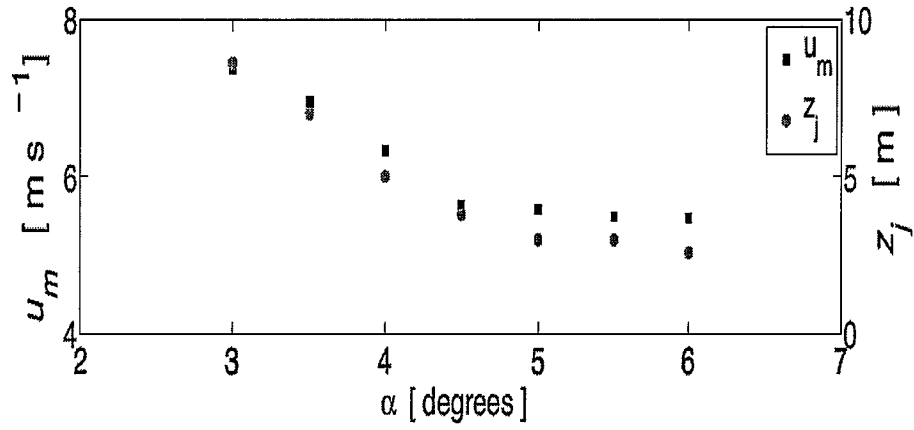
α [deg]	u_m [m s ⁻¹]	z_j [m]
3.0	7.36	8.6
3.5	6.96	7.0
4.0	6.33	5.0
4.5	5.64	3.8
5.0	5.58	3.0
5.5	5.50	3.0
6.0	5.48	2.6

The relation between Pr and the katabatic LLJ is described in Axelsen and Van Dop (2009a, b). They distinguish between Pr due to the resolved motions and that due to the subfilter scale model used in the LES (the latter dominates at the lowest model level and progressively becomes less important with height). Most of the resolved Pr values are ≈ 1 ; Pr generally increases with increasing gradient Richardson number (e.g. Kim and Mahrt, 1992; Zilitinkevich et al. 2008). The smallest resolved Pr values are found near the surface, $z < z_j$; the values gradually increase up to just below z_j and at z_j there is a discontinuity. Immediately above z_j large Pr values are obtained while higher up $Pr \approx 1$ again (Axelsen and Van Dop 2009b; their Fig. 4). Since the same LES model is used here (except for the description of the thermodynamic lower boundary condition, see Sec. 2), the same Pr behaviour is found here as well. Please note a stark difference in the treatment of Pr in the LES and classical model of Prandtl where Pr is a given constant.

The dependency of u_m and z_j on α is further examined in Figure 2. At low inclinations, $\alpha < 5^\circ$, u_m decreases gradually with increasing α , while z_j on the other hand, for larger slope angles, beyond $\approx 5^\circ$, the decrease in u_m is much weaker. Similar behaviour is found for the katabatic LLJ height as a function of

smaller.

245 the inclination; it is seen that $z_j = 8.6$ m for $\alpha = 3^\circ$, but it decreases to $z_j \approx 3$ m for $\alpha \geq 5^\circ$. Figure 2
 246 suggests a correlation between of u_m and z_j as functions of α , which is further explored in Figure 3.
 247



248
 249 **Figure 2.** The katabatic wind maximum u_m (black squares) and its height z_j (grey circles) as functions
 250 of the slope angle α obtained via LES model (the data from Figure 1 and Table 1).
 251

252 A linear regression, corroborating the results from Figures 2 and 3, yields

253

$$z_j = a u_m + b, \quad (6)$$

254

255
 256 with a correlation coefficient of 0.98.
 257

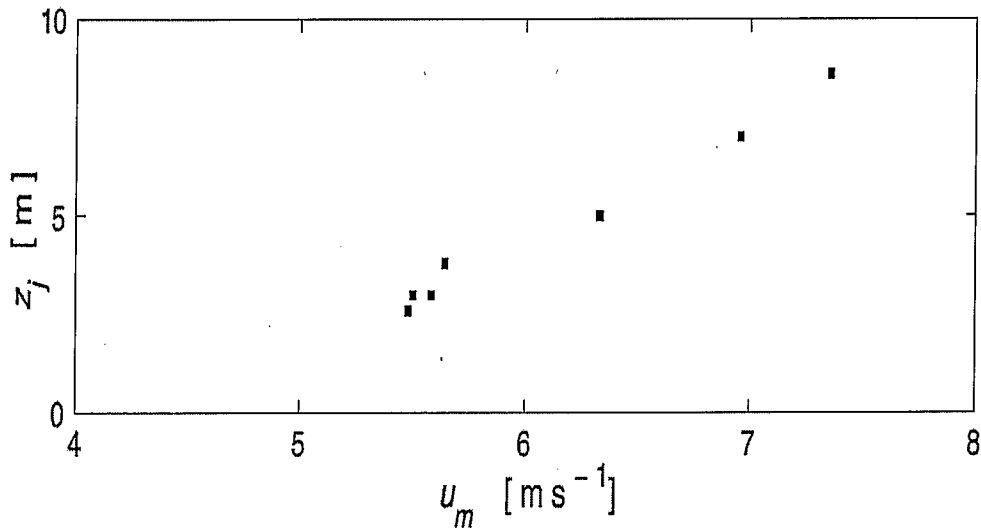


Figure 3. The katabatic wind maximum magnitude u_m versus its height z_j (the data from Figure 2).

Although it is unlikely that the linear relation holds for a significantly larger range of slope angles than the range used here, ^{Eg.} relation (6) is lent some support from measurements. Data from the PASTEX field campaign, taken over the Pasterze glacier, Austria (documented in e.g. Van den Broeke 1997), in which mast measurements and balloon soundings over a slope with inclination $\alpha \approx 5^\circ$ were collected, suggest that $z_j \approx 1.16 u_m$ with a correlation coefficient 0.78 (Oerlemans and Grisogono 2002; thier Fig. 7). In these measurements, the slope angle is nearly constant whereas the stratification of the ambient atmosphere and the surface temperature difference are variables. Therefore, the linear regression using the observational data, just like the regression obtained from the numerical results, is not necessarily valid for all slope inclinations. Different slope coefficients between a in (6) and that in the PASTEX data are most likely caused by idealized settings of the numerical simulations, e.g. a uniform slope, steady-state flow, no cross-slope winds and no large-scale pressure gradients. The observational data, on the other hand, were to a noticeable degree influenced by all of these factors (not shown), including some variations in the background stratification as well. We did not conduct ^a systematic analysis of the effects of aerodynamic roughness length changes on the LLJ; however, based on Axelsen and Van Dop (2009a, b), one should not expect ^a significant sensitivity of the LLJ for moderate variations of the aerodynamic roughness length range. In general, a larger aerodynamic roughness length should ^{more diffuse} somewhat lift the LLJ and ~~make it slightly more spread~~ ^{make it slightly more spread} in the vertical.

One of the main reasons that the LES results were averaged over the down-slope direction and time is a

more straightforward comparability with the results from the Prandtl model in the next sub-section. In this way, one wants to establish a sort of zeroth-order relationship between the LLJ maximum speed and height, and constant slope angle (the aim of this study). Further, higher-order and subtle effects will be dealt with in a future study including e.g. entrainment of potentially warmer air above the LLJ and the related drag, quasi-periodic LLJ pulsations pertaining to Kelvin-Helmholtz type of waves, which might trigger both internal (e.g. Chemel et al. 2009) and external buoyancy waves (Axelsen and Van Dop, 2009a; their Fig. 7a).

287

3.2. Prandtl model results

289

The obvious correlation between u_m and z_j found in our LES and mentioned for the PASTEX data (Oerlemans and Grisogono 2002) is not obtained from the classical Prandtl solution. The LES results show a nearly linear relation between u_m and z_j ; meanwhile, from (5) it can be found only that z_j is proportional to $\sin^{-1/2} \alpha$ whereas the magnitude of the wind ^{speed} maximum is independent of the slope inclination; hence, u_m/z_j is proportional to $\sin^{1/2} \alpha$ in the classical Prandtl model. The discrepancy between the ^{nonlinear} LES results and the explicit linear Prandtl solution ^{is} examined next in terms of the assigned constancy of Γ , K_H and Pr , in the classical Prandtl model.

297

First, the height of the Prandtl LLJ is found by differentiating (5) with respect to z . After a straightforward manipulation, $z_j = h\pi/4$, which is proportional to $\sin^{-1/2} \alpha$ (e.g. Grisogono and Oerlemans 2001b, their (4.3a)). Second, substituting this height in ^{to} (5), the maximum Prandtl speed ensues:

301

$$u_{m,P} = -C \left[\frac{g}{2\Theta_0 \Gamma Pr} \right]^{1/2} \exp(-\pi/4). \quad (7)$$

303

The main problem with (5), and thus (7), is that a) Γ does not sense the flow-induced, very strong, finite-amplitude vertical gradient of the potential temperature between the surface and the katabatic LLJ, and b) fixed and usually not well known Pr . ^{is used} Namely, Γ is usually considered as between 1 and 10 K km⁻¹, whereas the perturbed, i.e. flow-induced near-surface potential temperature gradient may easily exceed 10 K (20 m)⁻¹, see e.g. Grisogono and Oerlemans (2001b). Further up, say, $z > 2 z_j$, the

309 opposite, although weaker, thermal flow-induced effect occurs, which reduces the static stability of the
 310 flow, as seen qualitatively from (4), and supports a more efficient momentum mixing than below for z
 311 $\leq z_j$. This result also agrees with Chemel et al. (2009). Next, based on scaling arguments and trying to
 312 parametrize eddy diffusivities, the LLJ height behaves as $z_j \sim \Gamma \sin^{1/2}(\alpha)^{-1}$, where ^{the} minus sign
 313 indicates the opposite signs for z_j and C (since $C < 0$), ^{As} in Grisogono and Oerlemans (2001b; 2002)
 314 and Parmhed et al. (2004), relatively lower slopes yield higher z_j , which in turn, may allow for
 315 somewhat larger dominant eddies (though always smaller than z_j) and thus for a relatively weaker near-
 316 surface inversion than that for larger slopes.

317 ^{with the}
 318 As eddy diffusivity and conductivity, Pr should also be, in principle, a function of the flow, e.g. via ^{the}
 319 gradient Richardson number, as in Kim and Mahrt (1992), Zilitinkevich et al. (2008), Grisogono and
 320 Zovko Rajak (2009) and Grisogono (2010); ^H however, in this analytic model Pr remains constant for
 321 mathematical simplicity. Figure 4 corroborates the stated comments to the Prandtl model by
 322 comparing the LES wind maxima, for the smallest and largest slope angle considered (for simplicity),
 323 with the related wind profiles arrived at from the Prandtl solution. The latter is obtained with the
 324 equivalent input as in the LES results, Fig. 4a (with K_H and Pr ^{assumed,} ~~guessed,~~ expecting the diffusivity [?]
 325 values $< 0.5 \text{ m}^2 \text{ s}^{-1}$ and similar or smaller than those in Grisogono and Oerlemans 2001b). We do not
 326 change these input values in the Prandtl solution for the other slope considered, Fig. 4e, in order to
 327 preserve the simplicity and straightforward comparisons among the Prandtl particular solutions
 328 presented. In this way, it is easy to see various effects in the Prandtl wind [#] profile caused by a single
 329 input change. By inspection, one finds again the Prandtl solution for the maximum wind speed
 330 insensitive to the slope angle (compare the values of the speed maxima between the left and right
 331 column, for each row), but sensitive to both Γ and Pr as in (7).
 332

minus
sign

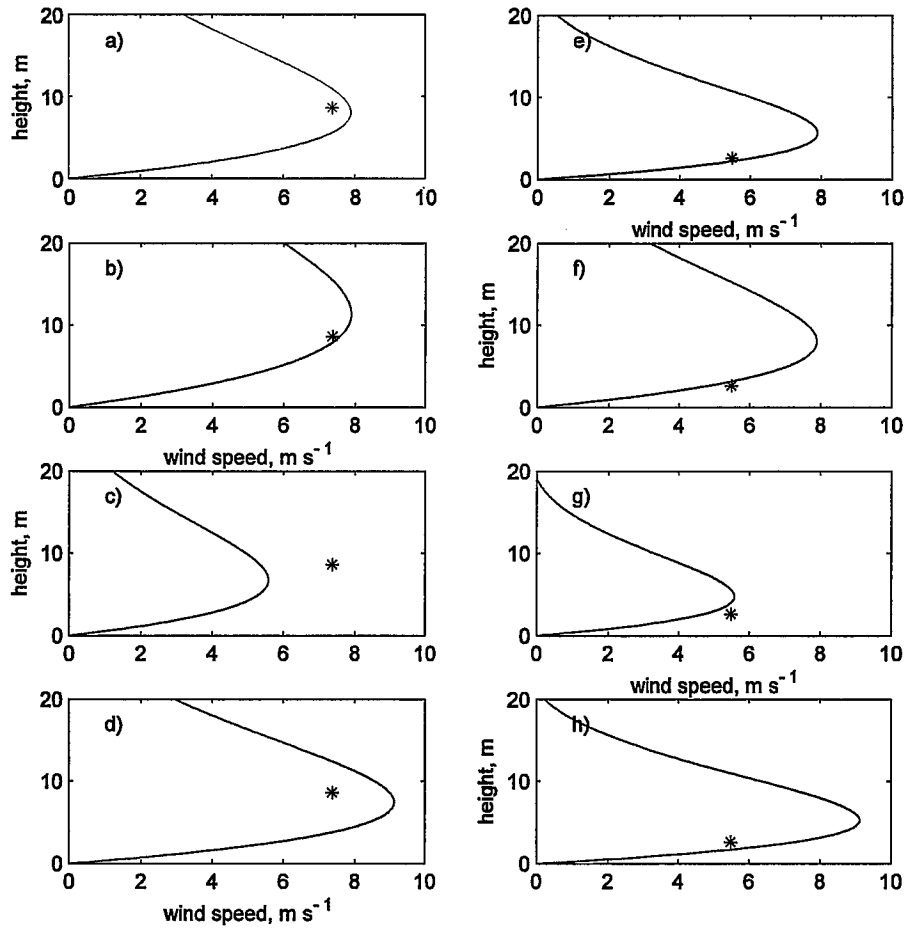
x

x

x

#

h



333

334 **Figure 4.** The Prandtl solution (solid) for the pure katabatic wind related to the former LES results (one
 335 star at each subplot showing the maximum of the katabatic LLJ): a) through d) slope angle $\alpha = 3^\circ$ and
 336 e) through h) $\alpha = 6^\circ$. All $K_H = 0.02 \text{ m}^2 \text{ s}^{-1}$ but in b) and f) where $K_H = 0.04 \text{ m}^2 \text{ s}^{-1}$; all $\Gamma = 3 \text{ K km}^{-1}$ but
 337 in c) and g) where $\Gamma = 6 \text{ K km}^{-1}$; all $Pr = 2$ but in d) and h) where $Pr = 1.5$. Particular results show
 338 (from above downward) the effect of doubling ^{the} eddy conductivity K_H (relatively small effect below the
 339 LLJ, stronger above it), background stratification Γ (significant effect), or lowering Prandtl number Pr
 340 (significant effect).

341

342 Perhaps somewhat counter-intuitively, the actual values of K_H or K_M are not directly responsible for
 343 the specific value of the maximum speed in the classical Prandtl model, but their ratio, i.e. Pr , has an
 344 equally important effect on the maximum speed as ^{does} Γ (also see Eq. 7). At the same time, values of the
 345 eddy diffusivities affect the overall shapes of (u, θ) profiles. Again, because it is linear, the classical

346 Prandtl model (see Eq. 3) does not take into account the flow perturbation effect, i.e. $\partial\theta/\partial z$ from (4), on
347 the background stratification, which can be important. Moreover, K_H and K_M are assigned as ~~guessed~~ *assumed*
348 constants.

349

350

351 4 Concluding remarks

352

353 The low-level jet (LLJ) of a pure katabatic flow over moderate slopes, ranging between 3 to 6°, is
354 assessed using LES and further discussed via the classical Prandtl model. We conclude from the LES

355 ^a results that for pure katabatic flow, both the maximum wind speed and its height decrease with ^a
356 ~~of the~~ steepening the slope; the classical Prandtl solution, due to the model linearity, accommodates only the

357 latter dependency (see Eq 7, while $z_j = \pi h/4$, that is proportional to $\sin^{-1/2}(\alpha)$). As shown in Figure 4,

358 the inability of the analytical Prandtl solution to give the maximum wind-speed dependency on the

359 slope angle is associated with the ^a assumed constancy, and thus ^a lack of interaction among: 1) the

360 background vertical potential temperature gradient Γ , 2) the eddy diffusivity, and 3) the Prandtl number

361 Pr . Meanwhile, in the LES the eddy diffusivity and conductivity respond to changes in stratification

362 and wind shear.

363

364 Although, a larger temperature gradient appears in the Prandtl model near the surface, it does not feed

365 back to the input stratification, eddy diffusivity and Pr . Since the dominant eddy size in the LES is

366 small compared to the LLJ height (because of the extremely strong near-surface static stability), the

367 vertical turbulent momentum flux vanishes at the LLJ nose and reverses its sign above the LLJ in

368 agreement with Van den Broeke (1997), Van der Avoird and Duynkerke (1999), Grisogono and

369 Oerlemans (2002), Oerlemans and Grisogono (2002), Cuxart and Jiménez (2007) and Axelsen and Van

370 Dop (2009a, b). Thus, the LLJ may effectively become decoupled from the rest of the flow and thus

371 become a robust and rather permanent feature of a cooled, inclined microclimate (Parmhed et al. 2004;

372 Cuxart and Jiménez 2007). We believe that our findings, linking the main properties of the katabatic

373 LLJ to the underlying slope, can be useful for parametrization improvements of katabatic flows in

374 NWP and climate models.

375

= constant α

376 For the lower slope angles, the katabatic steady-state flow is reached later than for the larger angle.
377 Moreover, because of $z_j \propto [T \sin^{1/2}(\alpha)]^{-1}$, ~~const~~ ^{with the constant} $\propto 0$, as in e.g. Parmhed et al. (2004), relatively
378 lower slopes yield higher z_j , which, in turn, may allow for somewhat larger dominant eddies (though
379 always smaller than z_j) and thus for a relatively weaker near-surface inversion than that for larger
380 slopes. Hence, the lower-angle flow accelerates for the longer time, deploying somewhat larger
381 dominant eddies below z_j and may acquire more momentum that is spread through deeper layers. In
382 contrast, the larger-angle flow accelerates for the relatively shorter time and accumulates less
383 momentum (using relatively smaller dominant eddies below z_j) that is spread through relatively thinner
384 layers, provided that only gentle slope angles are considered.

385
386 At significantly larger angles, which are not considered here, non-hydrostatic effects and wave
387 instabilities should play progressively more important roles; these would promote a more vigorous
388 momentum exchange than that considered here. On the contrary, for vanishingly small slope angles,
389 the wind ^h speed maximum cannot continue to increase, but it should ~~stop~~ ^{cease} increasing and eventually
390 decay to zero for zero slope angle. However, for zero slope angle the Prandtl model becomes invalid
391 (as discussed in Section 2), while the LES results become exceedingly expensive for reaching the
392 steady-state. Based on those last few plausible remarks, one may expect that there exist three different
393 slope-dependent regimes for pure katabatic winds; this study addressed ~~the one~~ ^{that} for moderate slopes.

394

395

396 Acknowledgements


397 Two anonymous reviewers are thanked for their efforts that led to an overall improvement of this note.
398 Han Van Dop and Hans Oerlemans are thanked for setting up ^{the} overall ^{work} scientific frame for this research
399 many years ago. The Faculty and Staff of IMAU, Utrecht ^U university, the Netherlands, are
400 acknowledged for the computing resources. B.G. is supported by the Croatian Ministry of Science,
401 Education & Sports, project BORA, No. 119-1193086-1311.

402

403

404 References

405

- 406 Axelsen SL, Van Dop H (2009a) Large-eddy simulation of katabatic winds. Part I: Comparison with
407 observations. *Acta Geophysica* 57(4): 803 – 836, DOI: 10.2478/s11600-009-0041-6
- 408 Axelsen SL, Van Dop H (2009b) Large-eddy simulation of katabatic winds. Part II: Sensitivity study
409 and comparison with analytical models. *Acta Geophysica* 57(4): 837 – 856, DOI: 10.2478/s11600-009-
410 0042-5
- 411 Burkholder BA, Shapiro A, Fedorovich E (2009) Katabatic flow induced by a cross-slope band of
412 surface cooling. *Acta Geophysica* 57(4): 923–949, DOI: 10.2478/s11600-009-0025-6
- 413 Chemel CC, Staquet A, Largeron Y (2009) Generation of internal gravity waves by a katabatic wind in
414 an idealized alpine valley. *Meteorol Atmos Phys* 103: 187-194
415
- 416 Cuxart J, Jiménez MA (2007) Mixing processes in a nocturnal low-level jet, an LES study. *J Atmos Sci*
417 64: 1666-1679
- 418 Denby B (1999) Second-order modelling of turbulence in katabatic flows. *Boundary-Layer Meteorol*
419 92: 67-100
- 420 Egger J (1990) Thermally forced flows: Theory. In W. Blumen, editor, *Atmospheric processes over*
421 *complex terrain*. Am Meteorol Soc 43-57 (323 pp) 
- 422 Esau IN (2004) Simulation of Ekman boundary layers by large eddy model with dynamic subfilter
423 closure. *J Environ Fluid Mech* 4: 273-303
- 424 Fedorovich E, Shapiro A (2009) Structure of numerically simulated katabatic and anabatic flows along
425 steep slopes. *Acta Geophysica* 57(4): 981-1010, DOI: 10.2478/s11600-009-0027-4
- 426 Grisogono B (2003) Post-onset behaviour of the pure katabatic flow. *Boundary-Layer Meteorol* 107:
427 157-175
- 428 Grisogono B (2010) Generalizing 'z-less' mixing length for stable boundary layers. *Q J R Meteorol*
429 *Soc* 136: 213-221
- 430 Grisogono B, Belušić D (2008) Improving mixing length-scale for stable boundary layers. *Q J R*
431 *Meteorol Soc* 134: 2185–2192
- 432 Grisogono B, Oerlemans J (2001a) Katabatic flow: analytic solution for gradually varying eddy
433 diffusivities. *J Atmos Sci* 58: 3349-3354

- 434 Grisogono B, Oerlemans J (2001b) A theory for the estimation of surface fluxes in simple katabatic
435 flows. *Q J R Meteorol Soc* 127: 2725 – 2739
- 436 Grisogono B, Oerlemans J (2002) Justifying the WKB approximation in pure katabatic flows. *Tellus*
437 54A: 453-463
- 438 Grisogono B, Zovko Rajak D (2009) Assessment of Monin-Obukhov scaling over small slopes.
439 *Geofizika* 26: 101-108, <http://geofizika-journal.gfz.hr/vol26.htm>
- 440 Haiden T (2003) On the pressure field in the slope wind layer. *J. Atmos. Sci.*, **60**, 1632-1635
- 441 Haiden T, Whiteman CD (2005) Katabatic flow mechanisms on a low-angle slope. *J. Appl. Meteorol*,
442 **44**, 113-126
- 443 Heilman W, Talke E (1991) Numerical simulation of the nocturnal turbulence characteristics over
444 Rattlesnake Mountain. *J Appl Meteorol* 30: 1106–1116
- 445 Kavčič I, Grisogono B (2007) Katabatic flow with Coriolis effect and gradually varying eddy
446 diffusivity. *Boundary-Layer Meteorol* 125: 377-387
- 447 Kim J, Mahrt L (1992) Simple formulation of turbulent mixing in the stable free atmosphere and
448 nocturnal boundary layer. *Tellus* 44A: 381-394
- 449 Largeron Y, Staquet C, Chemel C (2010) Turbulent mixing in a katabatic wind under stable conditions.
450 *Meteorol Z* 19: 467–480
- 451 Mahrt L (1982) Momentum balance of gravity flows. *J Atmos Sci* 39: 2701–2711
- 452 Oerlemans J, Grisogono B (2002) Glacier wind and parameterisation of the related surface heat flux.
453 *Tellus* 54A: 440–452
- 454 Oerlemans J, Björnson H, Kuhn M, Obleitner F, Pálsson F, Smeets CJJP, Vugts HF, De Wolde J
455 (1999) Glaciometeorological investigations on Vatnajökull, Iceland, summer 1996: An overview.
456 *Boundary-Layer Meteorol* 92: 3–26
- 457 Parish TR, Bromwich DH (1991) Continental-scale simulation of the Antarctic katabatic wind regime.
458 *J Clim* 4: 135–146
- 459 Parmhed O, Oerlemans J, Grisogono B (2004) Describing surface fluxes in katabatic flow on
460 Breidamerkurjökull, Iceland. *Q J R Meteorol Soc* 130: 1137–1151
- 461 Petkovšek Z, Hočevár A (1971) Night drainage winds. *Arch Meteor Geophys Bioklim* A20: 353-360

h.

- 462 Pielke RA (1984) *Mesoscale Numerical Modeling*. Academic Press, New York 612 pp
- 463 Prandtl L (1942) *Führer durch die Strömungslehre*. Vieweg und Sohn, 648 pp
- 464 Renfrew IA (2004) The dynamics of idealized katabatic flow over a moderate slope and ice shelf. *Q J R Meteorol Soc* 130: 1023–1045
- 466 Renfrew IA, Anderson PS (2006) Profiles of katabatic flow in summer and winter over Coast Land, Antarctica. *Q J R Meteorol Soc* 132: 779–802
- 468 Rotach M, Zardi D (2007) On the boundary-layer structure over highly complex terrain: Key findings from MAP. *Q J R Meteorol Soc* 133: 937–948
- 470 Schumann U (1990) Large-eddy simulation of the up-slope boundary layer. *Q J R Meteorol Soc* 116: 637–670
- 472 Shapiro A, Fedorovich E (2008) Coriolis effects in homogeneous and inhomogeneous katabatic flows. *Q J R Meteorol Soc* 134: 353–370
- 474 Smith CM, Skillingstad ED (2005) Numerical simulation of katabatic flow with changing slope angle. *Mon Weather Rev* 133: 3065–3080
- 476 Van den Broeke MR (1997) Momentum, heat, and moisture budgets of the katabatic wind layer over a midlatitude glacier in summer. *J Appl Meteorol* 36: 763–774
- 478 Van Dop H, Axelsen SL (2007) Large eddy simulation of the stable boundary-layer: A retrospect to Nieuwstadt's early work. *Flow Turb Combust* 79: 235–249
- 480 Van der Avoird E, Duynkerke PG (1999) Turbulence in a katabatic flow. Does it resemble turbulence in stable boundary layers over flat surfaces? *Boundary-Layer Meteorol.* 92: 39–66
- 482 Zhong S, Whiteman CD (2008) Downslope flows on a low-angle slope and their interactions with valley inversions. Part II: Numerical modeling. *J Appl Meteorol Climatol* 47: 2039–2057
- 484 Zilitinkevich SS, Elperin T, Kleorin N, Rogachevskii I, Esau I, Mauritsen T, Miles MW (2008) Turbulence energetics in stably stratified geophysical flows: strong and weak mixing regimes. *Q J R Meteorol Soc* 134: 793–799

